



# Graphene nanostructures toward clean energy technology applications

Xianfeng Zhang,<sup>1†</sup> Bin Wang,<sup>1†</sup> Jaka Sunarso,<sup>2</sup> Shaomin Liu<sup>3</sup> and Linjie Zhi<sup>1\*</sup>

Graphene, a one-atom-layer-thick carbon-structured material, has attracted global research attention due to its unique two-dimensional structure, high electrical conductivity, superior electron-transfer properties and charge-carrier mobility, large specific surface area, high transparency, and good mechanical properties. After its successful isolation into the free standing form in 2004, various graphene nanostructures have been developed and incorporated as key components in supercapacitors, lithium-ion batteries, solar cells, and fuel cells; the energy supporting devices which hold the key role to sustain our energy demand well into the future. Herein, we summarized the recent progress and performance of these graphene–nanostructure-based devices. © 2012 John Wiley & Sons, Ltd.

How to cite this article:

*WIREs Energy Environ* 2012, 1: 317–336 doi: 10.1002/wene.38

## INTRODUCTION

Energy supply and its supporting technology have rapidly emerged into an important research and development theme in the twenty-first century considering that constant global energy demand should be fulfilled in a sustainable way. The current primary energy resources, fossil fuel and coal, are already deemed environmentally incompatible; highly responsible for global warming effects, ozone layer depletion, biosphere and geosphere destruction, and ecological devastation.

Developing more efficient energy conversion technologies, large-capacity energy storage devices, and harnessing renewable energy devices are the primary objectives. In these respects, solar cells, fuel

cells, rechargeable lithium (Li)-ion batteries (RLBs), and electrochemical double-layer capacitors (EDLCs) are recognized as the best energy technologies with zero waste emission.<sup>1–10</sup> In all of these devices, however, electrode materials are the basic and essential component and generally determine their overall performances, efficiencies, and costs.

Graphene, a two-dimensional material with a single atomic thickness is the building unit for graphite. Since the first successful isolation of graphene in 2004,<sup>11</sup> its properties (e.g., room temperature quantum Hall effect,<sup>12</sup> optical properties,<sup>13</sup> mechanical properties, and thermoelectrical transport properties<sup>14</sup>) have been the subject of constant intensive investigation. Graphene is deemed well suited for electrochemical applications given that it provides many good properties such as high electrical conductivity, very large surface area, unique electron-transfer and charge-carrier mobility, high electrocatalytic activity, and high transparency.<sup>15–19</sup> Very recently, graphene and graphene-based materials have also been utilized as electrode materials in energy-related devices on which promising results were demonstrated.<sup>20–24</sup> The development of this area is so fast that significant progress has been achieved since our last review paper published at 2009.<sup>24</sup> This

<sup>†</sup>These two authors have contributed equally to the work.

\*Correspondence to: zhi@nanoctr.cn

<sup>1</sup>National Center for Nanoscience and Technology, Zhongguancun, Beijing, P. R. China

<sup>2</sup>Australian Research Council (ARC) Centre of Excellence for Electromaterials Science, Institute for Technology Research and Innovation, Deakin University, Burwood, Victoria, Australia

<sup>3</sup>Department of Chemical Engineering, Curtin University, Perth, Australia

DOI: 10.1002/wene.38

review intends to summarize the very recent status and progress in the application of graphene and graphene-based nanostructures inside clean energy supply and storage devices and their performances, including, particularly, EDLCs, RLBS, solar cells, and fuel cells.

## GRAPHENE NANOSTRUCTURES IN ELECTROCHEMICAL SUPER-CAPACITORS

In principle, electrochemical supercapacitors (ECs) can store energy by using either ion adsorption (EDLCs) or fast surface redox reactions (pseudocapacitors).<sup>25</sup> These power devices can be fully charged and/or discharged in seconds. Relative to batteries, they have lower energy density ( $\sim 5 \text{ Wh kg}^{-1}$ ) and a substantially larger power density ( $\sim 10 \text{ kW kg}^{-1}$ ). An EC cell is normally comprised of two porous carbon electrodes separated by a porous separator. The current collectors made from metal foil or carbon impregnated polymers are also included as the outermost layers to convey the electrical current from each electrode.

The superior energy density of the ECs (with respect to that of conventional capacitors) has been made possible by the very large specific surface area of the electrode material. For this purpose, the employment of nanomaterials with large surface area and high electric conductivity is crucial with the aim to enhance the EC performance. Currently, the core electrode materials are carbons, metal oxides, and conducting polymers, whereby activated carbon is by far the most commonly used material due to its superior conductivity and the high specific surface area. Most of the surface area in the activated carbon nevertheless arises from its interior pores, which unfortunately cannot be fully utilized in EC; in particular, pores with diameters smaller than 1 nm are inaccessible to the electrolyte.<sup>26</sup> No such problem, luckily, exists for graphene-based materials. More favorably, graphene demonstrates immense theoretical and practical advantages, such as excellent capacitance and low production costs.

The key pursued points to promote the performance of graphene in EC which relies largely on a double-layer capacitor principle is to enlarge the specific surface area by controllable layer stacking and distribution of the electrode material. Ruoff's group devoted great efforts in fabricating graphene-based EDLCs. They incorporated chemically modified graphene as electrode material for EDLC on which three electrolytes, namely, KOH, acetonitrile

and propylene carbonate were used which showed different performances.<sup>27</sup> The specific capacitance in KOH during charge at  $40 \text{ mV s}^{-1}$  scan rate remained almost constant at  $116 \text{ F g}^{-1}$  between 0.1 and 0.9 V. The specific capacitance in acetonitrile during discharge at  $20 \text{ mV s}^{-1}$  scan rate was  $100 \text{ F g}^{-1}$  from 1.5 to 0 V (fully discharged condition). The specific capacitance in propylene carbonate during discharge at  $20 \text{ mV g}^{-1}$  was  $\sim 95 \text{ F g}^{-1}$  from 2.0 to 0 V (fully discharged condition). Another innovation on the synthesis of graphene-based EDLC from Ruoff's group is the microwave assisted exfoliation and reduction of graphite oxide.<sup>28</sup> The thin crumpled and electronically conductive graphitic sheets were prepared via a simple and quick process in one minute. Using KOH as electrolyte, the specific capacitance of  $191 \text{ F g}^{-1}$  at  $150 \text{ mAh g}^{-1}$  discharge current was attained. Very recently, another work also reported that a porous carbon synthesized from graphene had a Brunauer–Emmett–Teller (BET) surface area of up to  $3100 \text{ m}^2 \text{ g}^{-1}$ .<sup>29</sup> This work hypothesized that this  $\text{sp}^2$ -bonded carbon possesses a continuous three-dimensional network of highly curved, atomic thick walls, leading to the formation of 0.6–5 nm width pores (Figure 1). The electrical conductivity of this carbon was quite high, whereas its O and H content were relatively low. The performance of this material in EDLCs was probed using a two-electrode symmetrical supercapacitor cell. The reported specific capacitance was 165, 166, and  $166 \text{ F g}^{-1}$  at current densities of 1.4, 2.8, and  $5.7 \text{ A g}^{-1}$ , respectively, with the corresponding volumetric capacitance of about  $60 \text{ F cm}^{-3}$  (Figure 2). Aside from these reported excellent performances, they claimed that the synthesis processes were readily scalable to industrial levels.

Using porous MgO layers as template, graphene that features one to two nanomesh-layered structure with specific surface area of up to  $1654 \text{ m}^2 \text{ g}^{-1}$  was synthesized on gram amount.<sup>30</sup> The obtained enlarged surface area with respect to graphene (graphene sheets are easily to stack and leads to severely reduced surface area) is claimed to be caused by the mass pores with diameter of  $\sim 10 \text{ nm}$ . The resultant uniform structures, in turn translate to excellent capacitance behavior in EDLC on which a specific capacitance of  $255 \text{ F g}^{-1}$  was obtained at  $10 \text{ mV s}^{-1}$  scan rate in 6 M KOH.

The existence of pores in graphene nanosheets (GNSs) tends to improve the specific surface area and thus enhance the capacitance of EC. Nevertheless, these pores also contribute to the increased resistance of the electrode, which is unfavorable for the transport of both electrons and ions. To this end, Miller

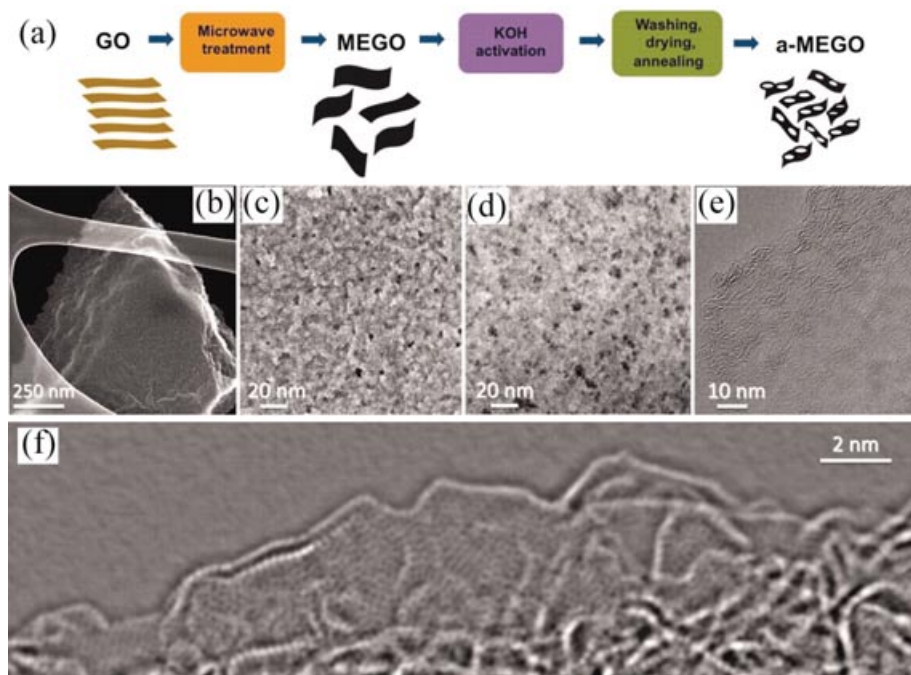


**FIGURE 1** | (a) Schematic pictures of the microwave exfoliation/reduction of the graphite oxide (GO) and the following chemical activation of microwave exfoliated graphite oxide (MEGO) with KOH which create pores whilst retain high electrical conductivity. (b) Low-magnification scanning electron microscopy (SEM) image of a three-dimensional a-MEGO piece. (c) High-resolution SEM image of a different sample region that demonstrates the porous morphology. (d) Annular dark field (ADF)-scanning transmission electron microscopy (STEM) image of the area in (c), acquired simultaneously. As observed, a-MEGO contains micro and mesopores with a size distribution between 1 nm and 10 nm. (e) High-resolution phase contrast electron micrograph on the thin edge of a-MEGO chunk, taken at 80 kV. There is a variation in focus across the image due to the sloped nature of the sample and changes in sample thickness. The image shows the presence of a dense network of nanometer-scale pores surrounded by highly curved, predominantly single-layer carbon. (f) Exit wave reconstructed high-resolution transmission electron microscopy (HR-TEM) image at the edge of a-MEGO. The in-plane carbon atoms are clearly resolved, and a variety of n-membered carbon rings is displayed. Substantial curvature of the single-carbon sheets is visible, with the in-plane crystallinity being preserved. (Reprinted with permission from Ref 29. Copyright 2011, AAAS.)

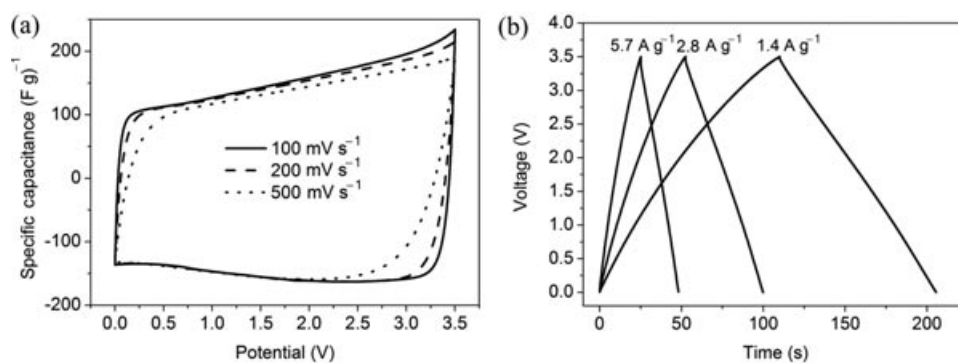


**FIGURE 2** | Supercapacitor performance of a-MEGO ( $SSA \sim 2400 \text{ m}^2 \text{ g}^{-1}$ ) in the BMIM  $\text{BF}_4/\text{AN}$  electrolyte. (a) CV curves at different scan rates. Rectangular shapes indicate the capacitive behavior. (b) Galvanostatic charge-discharge curves of a MEGO-based supercapacitor under different constant currents. (Reprinted with permission from Ref 29. Copyright 2011, AAAS.)

et al.<sup>31</sup> demonstrated efficient filtering of 120 Hz current with EC using electrodes made from vertically oriented GNSs grown directly on metal current collectors, as shown in Figure 3. In marked contrast with the typical resistance capacitor (RC) time of  $\sim 1$

second noted in normal EDLCs, this novel design demonstrates less than 200  $\mu\text{s}$  time attributed to the minimized electronic and ionic resistances. Moreover, unlike the normal designs, which rely on basal plane surfaces of graphene sheets, these graphene sheets

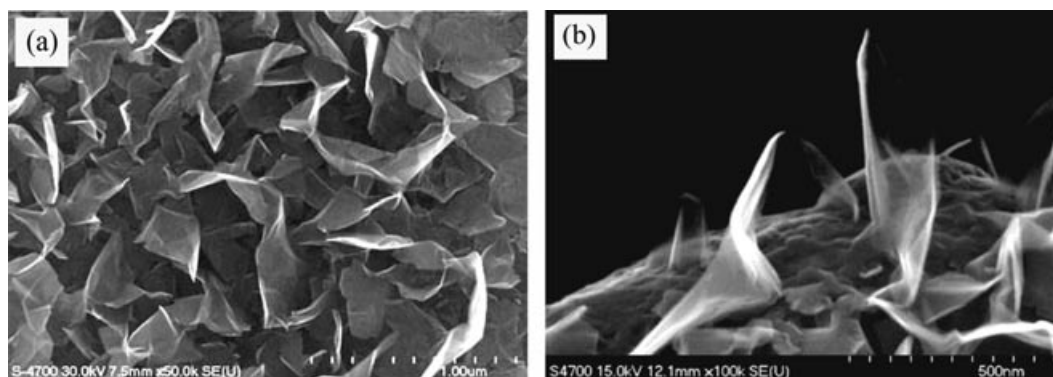


**FIGURE 3** | (a) Scanning electron microscopy (SEM) micrograph of coated Ni electrode. (b) SEM micrograph of a coated fiber, showing plan and shallow-angle views. (Reprinted with permission from Ref 31. Copyright 2010, AAAS.)

have a preponderance of exposed edge planes, which greatly improve the charge storage.

Typically, graphitic carbon-based materials are randomly oriented with respect to the current collectors in a conventional stacked geometry in ECs. As such, the electrolyte ions cannot penetrate into the far side of the graphitic planes, thus resulting in incomplete utilization of the electrochemical surface area of graphene layers.<sup>32</sup> To overcome this shortcoming, Yoo et al.<sup>32</sup> designed a novel thin-film energy device called ‘in-plane’ graphene EC, so that the surface of every graphene layer can be exploited more efficiently. The gravimetric capacitance of the active material attained from the device is  $247.3 \text{ F g}^{-1}$ . They have the opinion that the reported geometry can be easily extended to other thin-film-based EC and adapted to numerous structural and hybrid designs for energy storage devices.

Another reported strategy toward full utilization of the intrinsic surface capacitance and specific surface area of single-layer graphene was to prepare curved graphene sheets, which would not be restacked face to face.<sup>33</sup> When the sheets were packed and compressed into an electrode structure, a mesoporous structure was formed with a pore size in the range of 2–25 nm. A specific energy density of  $85.6 \text{ Wh kg}^{-1}$  at room temperature and  $136 \text{ Wh kg}^{-1}$  at  $80^\circ\text{C}$  (all based on the total electrode weight) was shown at a current density of  $1 \text{ A g}^{-1}$ . In comparison with the Ni metal hydride battery, it shows similar energy density but with much higher power density. The mesopore structure is also beneficial in terms of the upper limit potential attainment (up to 4 V) when ionic liquids are used as electrolytes.

Recently, self-assembled graphene and/or graphene oxide hydrogels attracted great attention.<sup>34,35</sup> Particularly, a great deal of effort has been devoted to exploring the applications of

these novel three-dimensional porous graphene networks in EDLCs.<sup>35–37</sup> The unique three-dimensional morphology allows most of the graphene sheets to be exposed to electrolyte, and provides open channels for the ionic diffusion. The fabricated EDLC showed a high specific capacitance of about  $200 \text{ F g}^{-1}$  at a low-discharge current density ( $0.3 \text{ A g}^{-1}$ ). Despite this, the capacitance decreased greatly at a high discharge rate, which was attributed to the low conductivity of the hydrogel. To improve the performance, a further study aiming to enhance the conductivity was performed by reducing the hydrogel with hydrazine and hydroiodic acid.<sup>36</sup> The chemically reduced hydrogel exhibited a higher specific capacitance of  $220 \text{ F g}^{-1}$  at  $1 \text{ A g}^{-1}$ . Interestingly, 74% of the capacitance could be maintained as the discharging current density was increased up to  $100 \text{ A g}^{-1}$ . Based on these results, the research went a step further by inviting pseudocapacitance into the graphene hydrogel. 2-Aminoanthraquinone (AAQ) molecules were covalently grafted onto graphene hydrogels for supercapacitor electrodes, and the capacitance reached  $258 \text{ F g}^{-1}$  at a discharge current density of  $0.3 \text{ A g}^{-1}$ .<sup>37</sup> The high performances of the graphene hydrogel-based supercapacitors make it promising for high rate charge–discharge applications.

Indeed, realizing mass production of individual graphene sheets is not an easy case. Nonetheless, some improvements and innovations have been demonstrated by these previous two works.<sup>32,33</sup> Furthermore, another method of intercalating conductive materials into the spacing between graphene layers to obtain separated graphene sheets has been reported. Carbon nanotubes (CNTs) and mesoporous carbon spheres were chosen to synthesize intercalated graphene composites.<sup>38,39</sup> For the first time, Fan et al.<sup>38</sup> prepared three-dimensional CNT/graphene sandwich structures with CNT pillars grown

in-between the graphene layers using chemical vapor deposition (CVD) approach. The BET surface area of this material is substantially higher relative to graphene, indicating the effective intercalation and distribution of CNTs in between the graphenes. The resultant CNT/graphene-based EC exhibits a specific capacitance of  $385 \text{ F g}^{-1}$  at  $10 \text{ mV s}^{-1}$  in  $6 \text{ M KOH}$ . After 2000 cycles, an increased capacitance ( $\sim 20\%$  of the initial capacitance) is noticed, highlighting excellent electrochemical stability of the electrode. Lei et al.<sup>39</sup> synthesized similar structure using mesoporous carbon spheres as the spacers and further measured the EC performance. They reported striking performance features, e.g., that the capacitance remains at 94% of the initial capacitance even after 1000 cycles of galvanostatic charge–discharge.

Nitrogen-doped graphene-based ECs exhibit comparable capacitances to those of utilizing pseudocapacitor principle yet featuring the robust charging mechanisms of ultracapacitors within the electrical double layers to the extent that excellent cycle lives are attained, thus fulfilling their inherent function as long-term energy storage devices.<sup>40</sup> In this case, Jeong et al.<sup>40</sup> fabricated ECs using nitrogen-doped graphene made from a simple plasma process. The obtained capacitance is  $\sim 280 \text{ F g}_{\text{electrode}}^{-1}$ , approximately four times of that shown by pristine graphene-based EC. Moreover, the device demonstrates excellent cycle life ( $>200,000$  cycles) and high power capability. It has also been reported that a human armband-shaped EC comprised of nitrogen-doped graphene, Ni, and conductive paper is able to power a light-emitting diode (LED).<sup>40</sup>

As previously mentioned, graphene exploits electrical double-layer capacitance effects as facilitated by its large specific surface area and electrical conductivity. As another capacitance contributing mechanism, pseudocapacitance can also contribute to the total capacitance, typically observed in active metal oxides such as  $\text{RuO}_2$ ,  $\text{NiO}_2$ , and  $\text{MnO}_2$ .<sup>41–44</sup> The significant drawback of such pseudocapacitors, however, is the limited cyclability of the electrodes. The breakthrough to achieve high power and high energy density hybrid ECs with long-cycle life seems to lie in the development of novel electrode materials, presumably through rational design of material combination, morphology, and size as well as proper choice of electrolytes which can support high voltages operation while featuring excellent ionic conductivity and electrochemical stability.<sup>44</sup> For this purpose, graphene (as a support and excellent electron transport media) in combination with transition metal oxides has been used to construct different nanostructures to achieve high-performance ECs.

By combining sol–gel and low-temperature annealing processes, Wu et al.<sup>41</sup> prepared hydrous ruthenium oxide ( $\text{RuO}_2$ )/graphene sheet composites, wherein the graphene sheets are well separated by fine  $\text{RuO}_2$  particles (5–20 nm). The fabricated ECs displays high specific capacitance of  $570 \text{ F g}^{-1}$  at 38.3 wt% Ru loading, excellent electrochemical stability (97.9% retention after 1000 cycles) and high energy density ( $20.1 \text{ Wh kg}^{-1}$ ) at low current rate ( $100 \text{ mA g}^{-1}$ ) and high power density ( $10,000 \text{ W kg}^{-1}$ ) at a reasonable energy density ( $4.3 \text{ Wh kg}^{-1}$ ). They argued that a synergistic effect of graphene and  $\text{RuO}_2$  was responsible for the excellent EC performance because the overall specific capacitance of the as-prepared composites was higher than the sum of specific capacitances of pure graphene and pure  $\text{RuO}_2$  in their relative ratios. Another similar design using nickel oxide nanoparticles as the active material was reported by Lv et al.<sup>42</sup> Membrane-like graphene/ $\text{NiO}$  hybrid materials with a layered sandwich nanostructure were prepared by a multistep assembly approach, which showed better electrochemical energy storage performance than the individual graphene membranes.

A promising way to allow the increased cell voltage and the energy density is to develop asymmetric ECs, which comprise a battery-type Faradaic electrode and a capacitor-type electrode to combine the advantages of both energy storage devices. A novel asymmetric EC device operated in neutral electrolyte using graphene/ $\text{MnO}_2$  and activated carbon nanofiber materials as the positive and negative electrodes, respectively was reported by Fan et al.<sup>43</sup> The graphene/ $\text{MnO}_2$  composites were synthesized by self-limiting deposition of nanoscale  $\text{MnO}_2$  on the surface of graphene under microwave irradiation. The asymmetric EC features favorable energy density ( $51.1 \text{ Wh kg}^{-1}$ ) and power density ( $198 \text{ kW kg}^{-1}$ ) as well as long cycle life (e.g., 97.3% specific capacitance was retained after 1000 cycles). Very recently, Yu et al. reported a solution-processed graphene/ $\text{MnO}_2$  nanostructured textile for high-performance EC.<sup>44</sup> In their protocol, graphene sheets were first coated on a three-dimensional, porous textiles support structures followed by electrodeposition of pseudocapacitive  $\text{MnO}_2$  nanomaterials on the textile. A specific capacitance of  $315 \text{ F g}^{-1}$  was obtained. Further on, asymmetric ECs were prepared using graphene/ $\text{MnO}_2$ -textile as the positive electrode and single-walled CNTs (SWNTs) textile as the negative electrode in an aqueous  $\text{Na}_2\text{SO}_4$  electrolyte solution. The attained power density of  $110 \text{ kW kg}^{-1}$  and an energy density of  $12.5 \text{ Wh kg}^{-1}$  seem to be lower relative to those obtained in Fan and co-workers' work,<sup>43</sup> yet the demonstrated cycling performance (e.g.,  $\sim 95\%$

capacitance retention over 5000 cycles) is substantially better.

To summarize, the recent advances in graphene-based ECs include complete utilization of the specific surface area of graphene, fabrication of graphene-based flexible or portable EC devices and asymmetric ECs including utilization of graphene as additives in ECs. There is no doubt that graphene will be the core material in the future ECs and that the nanoarchitecture will play a key role in developing high-performance energy storage devices.

## GRAPHENE NANOSTRUCTURES IN LITHIUM-ION BATTERIES

Lithium-based rechargeable batteries offer high energy density and small size and therefore have emerged as the most common power sources for portable electronics.<sup>45</sup> Needless to say that although every component of the battery (e.g., cathode, anode, and electrode) are crucial and has kept attracting great research attention till recent years, the electrode particularly cathode materials largely determines the overall cell performance. The intercalation of  $\text{Li}^+$  in cathode materials proceeds by the simultaneous insertion of  $\text{Li}^+$  ions in cathode's crystal lattices and reduction of the transition metal ion (the latter to satisfy the compound's electricity neutrality criterion). For anodes, upon charging,  $\text{Li}^+$  ions that come from cathode materials will pass through the electrolyte and intercalate into the anode to form  $\text{Li}/\text{C}$  or alloy structures.<sup>24</sup> Upon discharging, the process is reversed. To comply with the industrial requirements in terms of safety, volumetric density, coulombic efficiency, and cycle life, bulk particles have been used to fabricate the electrodes. Nonetheless, a challenge remains to scale up Li-ion batteries (LIB) for more demanding applications such as in hybrid electric vehicles, considering the presumed excessive polarization at high charge–discharge rates and low power density for this battery type.<sup>46</sup> In this regard, controlling nanostructure of the electrode materials to increase the  $\text{Li}^+$  transport rate in the solid phase has become popularized to achieve novel energy storage devices having both high energy density and high power density.

Graphene has already displayed its great potential by replacing conventional anode materials due to its higher specific capacities and higher power densities. Graphene is also beneficial in terms of its high coulombic efficiency (the ratio of the extracted Li to the inserted Li), allowing reversibly charging–discharging intercalation process at low potentials,

which translates into a high specific capacity. In addition, graphene's two-dimensional edge plane sites aids in Li-ion adsorption and diffusion, resulting in reduced charging period and increasing power outputs. The very large specific surface area of graphene not only increases the available interfaces for interaction with  $\text{Li}^+$  (the solid electrolyte interphase (SEI) increased as well) yet acts as good base platform to form composites with other active materials. Therefore, large amount of works have been focused on the nanostructure control and development of intrinsic graphene-based electrode materials and graphene composites for LIB.<sup>47–61</sup>

Theoretical calculation suggests that every six carbon atoms can only host one Li ion to form a  $\text{LiC}_6$  structure when Li ions are intercalated into the graphene layers of anode graphite, resulting in a maximum theoretical capacity of  $372 \text{ mAh g}^{-1}$  for graphite. As graphene layers are stacked orderly in graphite with layer spacing of 0.334 nm, fully exfoliated graphene layers can afford much higher capacity than graphite because Li ions can be stored on the two sides of one graphene layer. The arrangement and morphology of graphenes in the material might thus influence significantly the anode electrochemical performance. To this end, controlling the intergraphene sheet distance by modifying the graphene preparation procedures and/or through interaction with molecules such as CNTs or fullerenes ( $\text{C}_{60}$ ) have been pursued.

Reduction of graphene oxide is a common method to synthesize graphene materials. Wang et al.<sup>47</sup> use this procedure to synthesize GNSs in large quantities with special morphologies. The GNSs agglomerated and crumpled naturally into shapes resembling flower petals (Figure 4). The electrochemical properties of the curved graphene sheets (as anodes in LIB) were evaluated using constant current charge–discharge cycling at 0.02–0.03 V and 1 C rate. A reversible capacity of  $650 \text{ mAh g}^{-1}$  was obtained. They proposed that the Li ions are adsorbed on both sides of the graphene sheet, which were arranged like a 'house of cards' in hard carbons, leading to two layers of Li for each graphene sheet and a theoretical capacity of  $744 \text{ mAh g}^{-1}$  (by forming  $\text{Li}_2\text{C}_6$ ).<sup>48,49</sup> Thus the as-prepared graphene allows larger capacity comparable to that for highly exfoliated graphene materials.

Electrochemical exfoliation of graphite is a novel process to prepare graphene materials. The exfoliated graphitic platelets exhibit different morphology and size with respect to the graphite and graphene sheets and has also been employed as the anode material in LIB.<sup>50</sup> The graphitic platelets are of submicron thickness and show similar lattice structure with

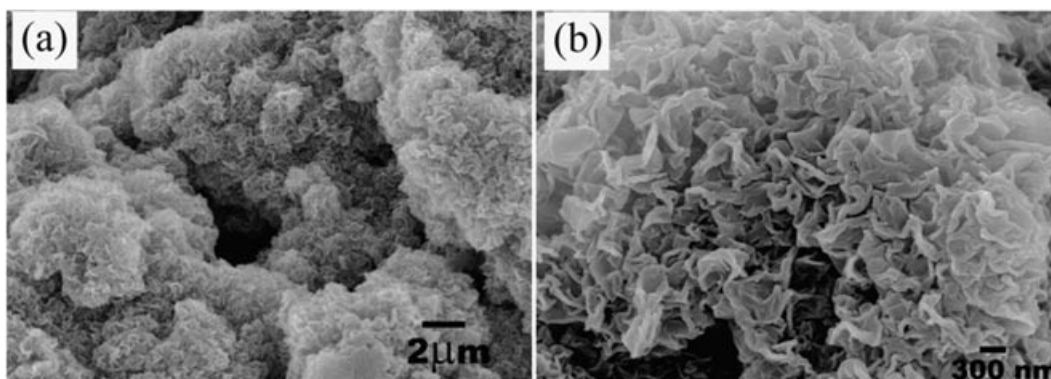


**FIGURE 4** | (a) Low-magnification FEG-SEM image of loose graphene nanosheet (GNS) powders. (b) High-magnification FEG-SEM view of GNS petals. (Reprinted with permission from Ref 47. Copyright 2010, Elsevier.)

the original graphite. The attained reversible capacity was similar to that of graphite with better rate capability. For example, substantial capacity reduction was not noticed at higher charge rates of 3 C and 5 C (relative to the capacity at 1 C). The shortened  $\text{Li}^+$  diffusion distance and well-defined lattice structure were argued to be the main responsible factors. The novel graphitic material might thus complement the common graphite and graphene and be considered further as a potential anode material for LIB.

Although the intrinsic monolayer graphene might enable high theoretical capacity, it is deemed difficult to synthesize fully exfoliated GNSs without any additions. In one recent study, a graphene-based electrode using CNTs and  $\text{C}_{60}$  as spacers to prevent the restacking of the graphene sheets was fabricated.<sup>51</sup> The reversible capacity of graphene, graphene/CNTs, and graphene/ $\text{C}_{60}$  materials were shown to be significantly altered as a function of the d-spacing of the GNSs. The modified electrodes showed a specific capacitance of 540, 730 and 784  $\text{mA h g}^{-1}$  for graphene, graphene/CNTs and graphene/ $\text{C}_{60}$  materials, respectively. This result demonstrates that the expansion in the d-spacing between graphene sheets obtained through combining some spacers seems to create additional sites to accommodate Li ions. Another innovation proposed by Fan and colleagues to optimize the graphene structure might also be used for LIB applications.<sup>30</sup> A three dimensional CNTs/graphene sandwich structure with CNT pillars grown in between the graphene layers can be prepared using CVD. This unique structure is expected to allow higher ion transport rate and full independence between each thin layer graphenes. Yang et al.<sup>52</sup> successfully fabricated nano-graphene-based hollow carbon spheres with dual shell-exterior mesoporous shells containing perpendicular nanochannels and interior graphitic solid shells (Figure 5). As anode material

for LIB, a reversible capacity of  $\sim 600 \text{ mAh g}^{-1}$  and high-rate capability of  $\sim 200 \text{ mAh g}^{-1}$  at the 10 C rate were shown.

Increasing the specific surface area of graphene materials is effective toward improving the capacity of LIB yet the simultaneous formation of larger SEI layer substantially reduces the coulombic efficiency. To prevent the latter, another procedure to improve the intrinsic specific capacity of graphene by doping graphene with nitrogen or boron has been reported.<sup>53</sup> High power and high energy density LIB under high-rate charge and discharge conditions was successfully fabricated using doped graphene as anode materials. The doped graphene shows a high reversible capacity in excess of  $1040 \text{ mAh g}^{-1}$  at a low rate of  $50 \text{ mA g}^{-1}$  which is superior to that shown by natural graphite. Moreover, the device allows fast charging ( $\sim 1 \text{ h}$  to several tens of seconds). For instance, a capacity of  $235 \text{ mAh g}^{-1}$  was attained using boron-doped graphene at  $25 \text{ A g}^{-1}$  rate (requires  $\sim 30 \text{ s}$  for complete charge). The excellent performance was claimed to be attributed to the unique structure of the graphene and the additional active dopants. Nonetheless, the detailed contributing mechanisms of additional atoms specifically on their interaction with Li ions are not clear yet.

Because the interaction of intrinsic graphene and Li ions is restricted in accordance with the  $\text{Li}_2\text{C}_6$  formation, the upper limit of graphene' specific capacity is expected to be lower relative to several inorganic materials, regardless of any performed modification. On another note, anode materials with superior capacities such as Li, Si,  $\text{SnO}_2$ , and  $\text{Mn}_3\text{O}_4$  normally exhibit safety issues related with excessive reactions. For example, large volume change ( $\sim 300\%$ ) occurred on  $\text{SnO}_2$  during charge-discharge process; causing electrode crumbling and cracking and electrical disconnection from the current

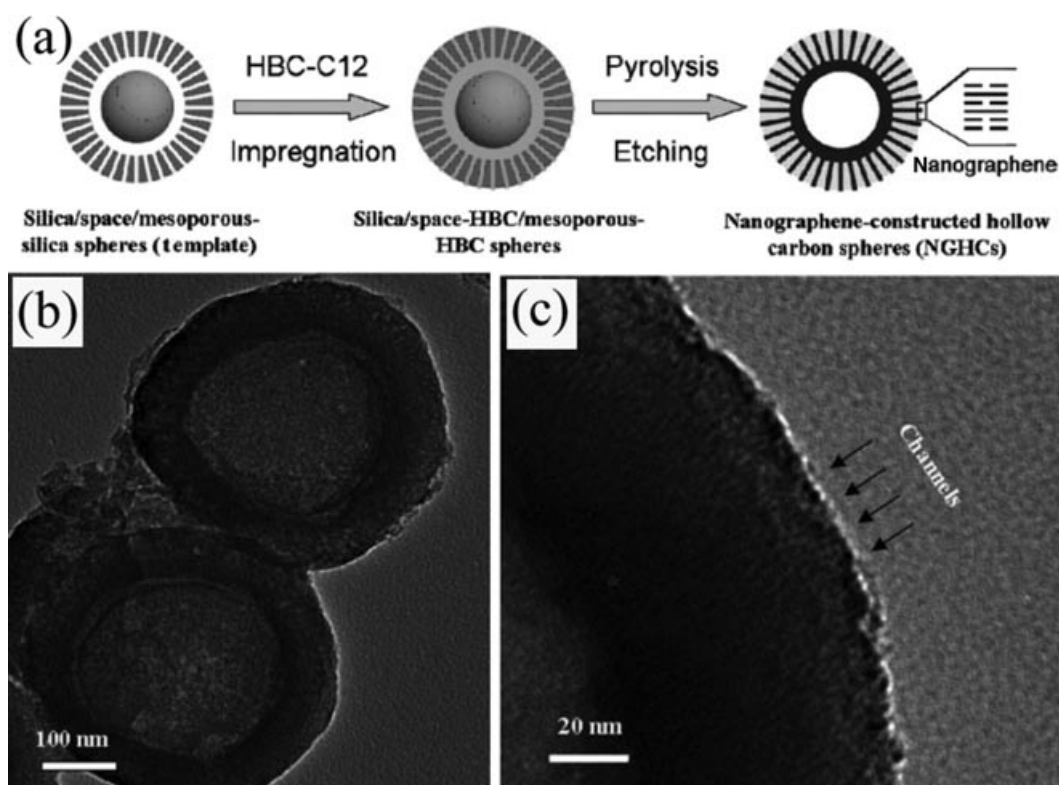


**FIGURE 5** | (a) Schematic illustration of the fabrication of nano-graphene-based hollow carbon spheres. (b, c) Transmission electron microscopy images of nano-graphene-based hollow carbon spheres. In the exterior walls of NGHCs, nanochannels arrange perpendicularly to the surface of curved spheres which is favorable for lithium-ion diffusion from different orientations; the interior graphitic solid walls also facilitate the collection and transport of electrons during the cycling process. (Reprinted with permission from Ref 52. Copyright 2009, John Wiley and Sons, Ltd.)

collectors.<sup>54</sup> Here, it might be attractive to employ the composite concept whereby the advantages of both graphene and these reactive electrode materials can be combined.

Kumar et al.<sup>50</sup> synthesized Li-intercalated graphene sheets via the reduction of exfoliated graphene oxide in liquid ammonia and Li metal. The lithiated graphene oxide was used as an anode material and provided better performance with respect to the commercially available graphite electrode. Although the preintercalation of Li ions into anode leads to enhanced performance, the battery capacity seems to be reduced. Probably, the most attractive features obtained by incorporating graphene into reactive electrode materials are the improved cyclability and electron conduction. SnO<sub>2</sub>/graphene nanoporous electrode was made by Paek et al.<sup>54</sup> on which a reversible capacity of 810 mAh g<sup>-1</sup> was demonstrated in the resultant LIB device. The device also has a long cycle lifetime as evidenced by 70% retaining of the initial capacity after 30 cycles. This is of marked improvement relative to the SnO<sub>2</sub> nanoparticles. Similarly, the dimensional confinement of tin oxide nanoparticles by the surrounding graphene may limit the

volume expansion, which occurs during Li insertion to the extent that the created pores between SnO<sub>2</sub> and graphene could be used as buffer spaces during charge–discharge to sustain favorable cyclic performances.

Combining reactive electrode materials with carbonaceous materials have been widely utilized to improve the cycle performances of reactive electrode material-based LIBs. Graphene with high electrical conductivity and sufficient ductility is of particular interest here. Nonetheless, the traditional problem of these graphene composites lies in is the aggregation of metal and metal oxides. Here, confining their aggregation, using individual graphene sheet, seems promising.<sup>55–57</sup> Yang et al.<sup>58</sup> reported the fabrication of graphene-encapsulated oxide nanoparticles with well-defined structures and further investigated the performance of LIB based on the resultant graphene/Co<sub>3</sub>O<sub>4</sub> electrode material. They demonstrated remarkable Li storage performance in terms of high capacity (~1100 mAh g<sup>-1</sup> during the initial 10 cycles) and excellent cycle performance (~1000 mAh g<sup>-1</sup> after 130 cycles).

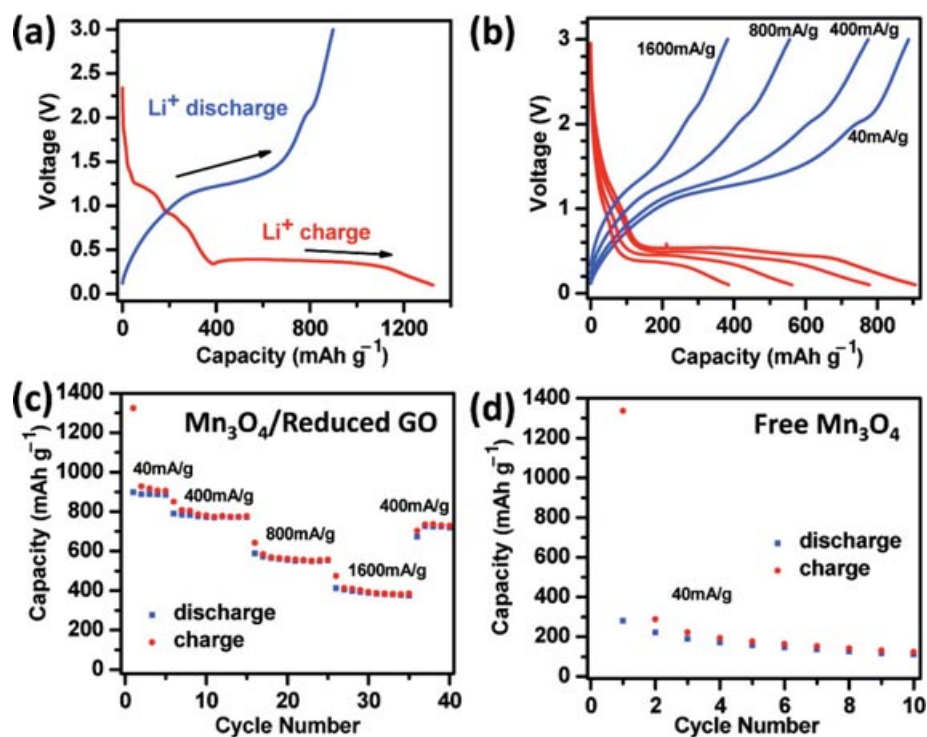


**FIGURE 6** | Electrochemical characterizations of a half-cell composed of  $\text{Mn}_3\text{O}_4/\text{RGO}$  and Li. The specific capacities are based on the mass of  $\text{Mn}_3\text{O}_4$  in the  $\text{Mn}_3\text{O}_4/\text{RGO}$  hybrid. (a) Charge (red) and discharge (blue) curves of  $\text{Mn}_3\text{O}_4/\text{RGO}$  for the first cycle at a current density of  $40 \text{ mA g}^{-1}$ . (b) Representative charge (red) and discharge (blue) curves of  $\text{Mn}_3\text{O}_4/\text{RGO}$  at various current densities. (c) Capacity retention of  $\text{Mn}_3\text{O}_4/\text{RGO}$  at various current densities. (d) Capacity retention of free  $\text{Mn}_3\text{O}_4$  nanoparticles without graphene at a current density of  $40 \text{ mA g}^{-1}$ . (Reprinted with permission from Ref 59. Copyright 2010, American Chemical Society.)

Wang et al.<sup>59</sup> developed a two-step solution-phase reaction to synthesize  $\text{Mn}_3\text{O}_4$  nanoparticle/reduced graphene oxide (RGO) hybrid. The selective growth of  $\text{Mn}_3\text{O}_4$  nanoparticles onto the RGO sheets (unlike free particle growth in solution) enables the electrically insulating  $\text{Mn}_3\text{O}_4$  nanoparticles to be *wired-up* to a current collector through the underlying conducting graphene network. The hybrid material exhibited a high specific capacity up to  $900 \text{ mA h g}^{-1}$ , near the theoretical capacity of  $\text{Mn}_3\text{O}_4$  ( $936 \text{ mA h g}^{-1}$ ) with a good rate capability and cycling stability (a capacity of  $730 \text{ mA h g}^{-1}$  at  $400 \text{ mA g}^{-1}$  was retained after 40 cycles). Without graphene presence,  $\text{Mn}_3\text{O}_4$  nanoparticles synthesized using the same process showed inferior performance. For example, at a low current density of only  $40 \text{ mA g}^{-1}$ , the  $\text{Mn}_3\text{O}_4$  nanoparticles showed a capacity lower than  $300 \text{ mA h g}^{-1}$  which decreased further to  $115 \text{ mA h g}^{-1}$  after 10 cycles (Figure 6).

Graphene composites such as graphene/ $\text{LiFePO}_4$  and graphene/sulfur can also be used as cathode materials.<sup>60,61</sup> Very recently, through wrapping poly (ethylene glycol)-coated submicron sulfur particles with mildly oxidized graphene oxide sheets decorated by carbon black

nanoparticles, Wang and colleagues<sup>63</sup> synthesized graphene/sulfur composite for cathode material application. This material is developed to resolve several existing problems in Li-S batteries because sulfur has high theoretical specific capacity of  $1672 \text{ mA h g}^{-1}$  as cathode.<sup>62,63</sup> Still, practical development of Li-S batteries is currently hindered by many problems such as sulfur's low electrical conductivity, dissolution of polysulfide in electrolyte, and significant sulfur volume expansion during discharge.<sup>61</sup> The uniform structure of graphene/ $\text{Co}_3\text{O}_4$  previously demonstrated by Yang et al.<sup>58</sup> can also be reproduced in graphenes encapsulated sulfur particles for use as cathode materials. They proposed that the coating layers were crucial to accommodate the volume expansion of the coated sulfur particles during discharge and to trap soluble polysulfide intermediates as well as to contribute toward the electrical conductivity. Indeed, after 100 cycles, the specific capacity was maintained at  $\sim 600 \text{ mA h g}^{-1}$  denoting its promise as cathode in LIB.

So far, it can be clearly noted that the presence of graphene by itself or in conjunction with other materials to form composites are beneficial and lead to enhanced electrochemical properties over the

reactive electrode materials, particularly in terms of the specific capacity and performances over increasing cycles. Graphene seems to hold an imminent role in the future development of this device. Most likely, the graphene-based composite wherein the graphene acts as additives, instead of the carbon materials would be of substantial role in the next generation LIB devices featuring high energy and power density.

## APPLICATIONS OF GRAPHENE IN SOLAR CELLS

Solar energy is a clean renewable energy resource, which can be directly converted into electricity by photovoltaic devices. Graphene has also found its use in numerous related applications, e.g., transparent electrodes, dye-sensitized and heterojunction solar cells.<sup>23,24,64–66</sup>

Window electrode is a key part in most solar cells. Presently, indium tin oxide (ITO) and fluorine tin oxide (FTO) are the benchmark window electrodes in solar cells.<sup>67</sup> Nonetheless, several associated drawbacks exist and limit their efficiency and wide utilizations, namely, (1) limited indium resource on

earth, (2) ionic diffusion from ITO to polymer layers in organic solar cell, (3) poor transparency in the near infrared region, and (4) instability of ITO at acid or base conditions.<sup>68,69</sup> In addition, the fact that ITO is brittle further restricts its application in flexible organic photovoltaics.<sup>70</sup> Thus, alternative window electrode which is cheap, easily available and featuring good performance is warranted. Compared to metal oxides, graphene is more appropriate as alternative window electrode in terms of its electronic conductivity and two-dimensional structures. Moreover, graphene might have high transparency considering its very thin atomic layer. To this end, graphene has been mixed with polymers<sup>71</sup> or silica<sup>72</sup> to prepare conductive composites. The conductivity of the resultant composite materials, unfortunately, is quite low, rendering their impracticality as electrode in optoelectronic devices. Very recently, we used exfoliated graphite oxide as starting material followed by film deposition and thermal reduction to obtain graphene films with a transparency of higher than 70% and a conductivity of several hundred  $S\text{ cm}^{-1}$ , as shown in Figure 7.<sup>68</sup> For the first time, dye-sensitized solar cells were made utilizing graphene film as window electrode. This result, in turn, provides an additional

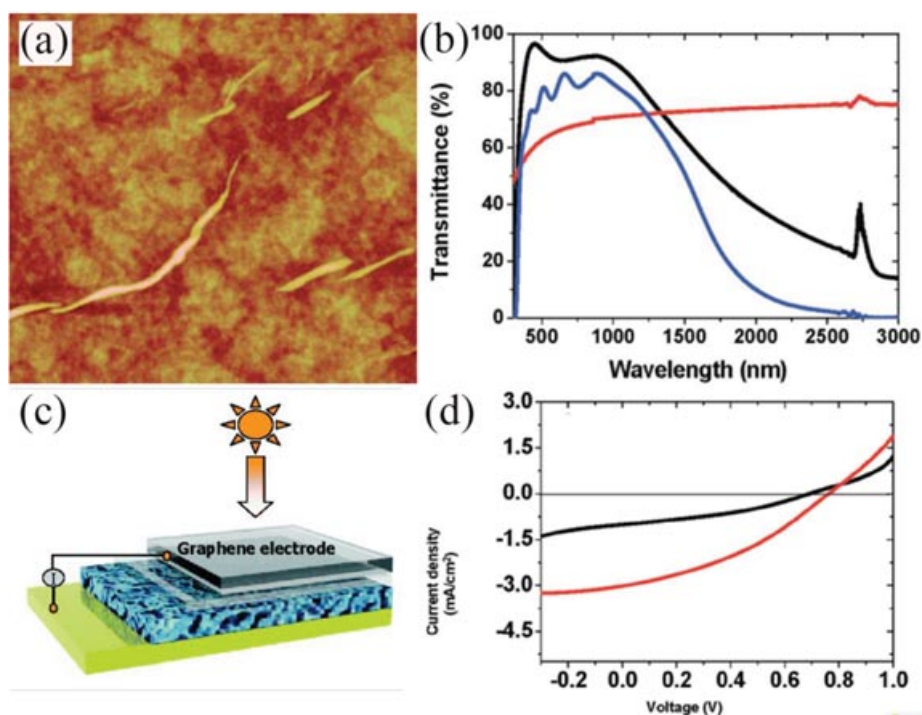


**FIGURE 7** | Graphene films, as an alternative to the metal oxides window electrodes for solid-state dye-sensitized solar cells. (a) Atomic force microscopy (AFM) height image of graphene films ( $\sim 10\ \mu\text{m}^2$ ). (b) Transmittance of a ca. 10 nm thick graphene film (red), in comparison with that of indium tin oxide (black) and fluorine tin oxide (FTO) (blue). (c) Illustration of dye-sensitized solar cell using graphene film as electrode, the four layers from bottom to top are Au, dye-sensitized heterojunction, compact  $\text{TiO}_2$ , and graphene film. (d)  $I$ - $V$  curve of graphene-based cell (black) and the fluorine-tin-oxide-based cell (red). (Reprinted with permission from Ref 68. Copyright 2008, American Chemical Society.)

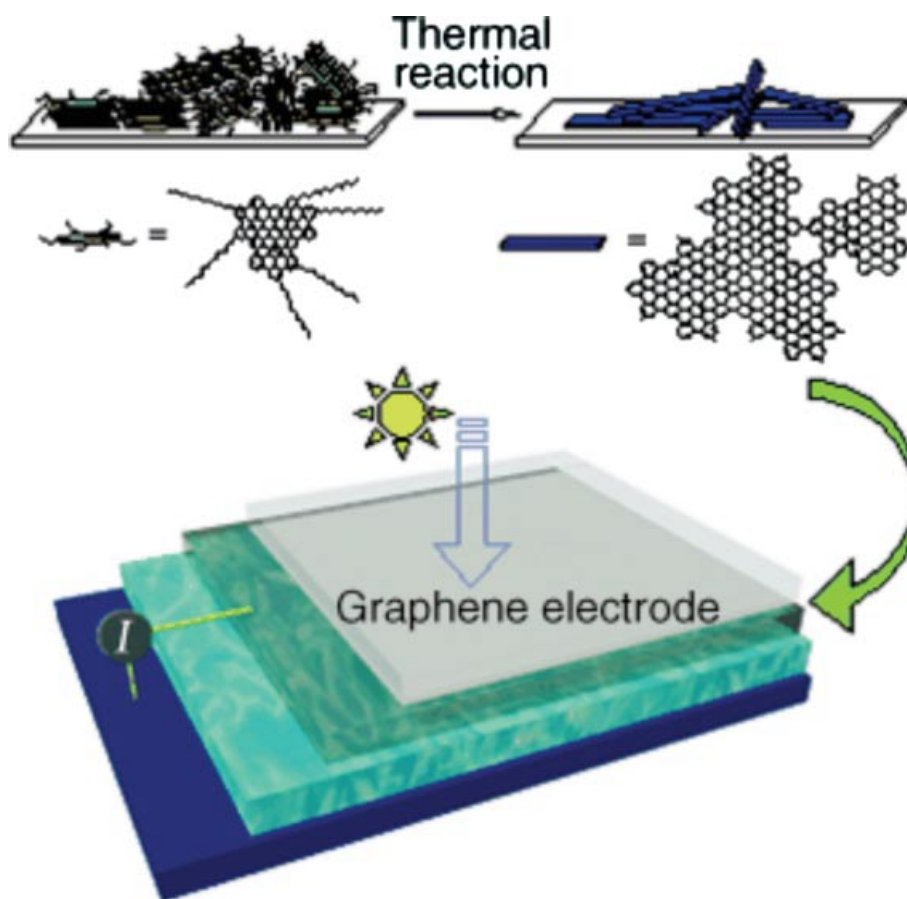


**FIGURE 8** | A transparent graphene film with 85% transparency obtained by a bottom-up chemical approach involving the thermal reaction of synthetic nanographene molecules of giant polycyclic aromatic hydrocarbons which are cross-linked with each other and further fused into larger graphene sheets. Such graphene films were applied as window electrodes in organic solar cells. The four layers of the solar cell illustration, from bottom to top are Ag, a blend of P3HT and PCBM, TGF, and quartz, respectively. (Reprinted with permission from Ref 69. Copyright 2008, John Wiley and Sons, Ltd.)

motivation to search alternative window electrode aside from ITO and FTO.

The interaction of graphene and the substrates was reported to be enhanced by choosing specific graphene precursors. Graphene films prepared via the self-assembly of discotic giant polycyclic aromatic hydrocarbons and further thermal cross-linking on transparent substrates demonstrated high stability on processing even in solution.<sup>69</sup> The property of graphene film was improved by this bottom-up approach using a monodispersed molecular nanographene as building units. The prepared graphene film showed stronger interactions with the substrate than that of graphite oxide induced film. The 4 nm thick film has a transparency of 90% at a wavelength of 500 nm. Accordingly, the solar cells were successfully fabricated incorporating such graphene film electrode with 85% transparency. Under the illumination of the simulated solar light,

the cell with graphene and ITO as electrode materials showed an overall efficiency of 1.17% and 0.29%, respectively.<sup>69</sup> Organic solar cells based on these graphene electrodes can be easily fabricated, as shown in Figure 8.

Graphene film prepared by spin coating of graphite oxide on quartz slice followed by subsequent reduction were used as window electrode in solar cell by Chen et al.<sup>69,73</sup> Atomic force microscopy (AFM) results showed that the film thickness was less than 10 nm with the surface roughness of  $\sim 3$  nm. The film transparency was in excess of 80% when the film thickness was less than 20 nm, whereas the film resistance ranged between 5 k $\Omega$  to 1 M $\Omega$ . The organic solar cell incorporating this graphene film as electrode exhibited a power conversion efficiency (PCE) of 0.4%, lower than that of the cell incorporating ITO electrode (0.84%); probably due to the larger resistance of the graphene film.

Graphene film with large area was synthesized on Ni-coated SiO<sub>2</sub>/Si wafer using a CVD process.<sup>74</sup> On 6–30 nm thick graphene film, the average sheet resistance varied from 1350 to 210 Ω sq<sup>-1</sup>, which was lower than that of chemically fabricated graphene oxide films by a factor of 2–3. The graphene film was then utilized as an anode in the organic photovoltaic device. The obtained  $V_{oc}$ ,  $J_{sc}$ , and FF were 0.32 V, 2.39 mA cm<sup>-2</sup> and 27%, respectively. These parameter values indicate that the cell performs poorly most probably due to the hydrophobic property of graphene, which leads to the nonuniform coating of polystyrenesulfonate-doped poly(3,4-ethylenedioxythiophene) (PEDOT:PSS). To improve the surface wettability, the graphene anode was then modified by UV/ozone treatment, resulting in higher PCE of 0.74%. Accordingly, noncovalent functionalization with pyrene buanoic acid succidymidyl ester (PBASE) was trialed to modify graphene. The solar cell using a PBASE-modified graphene anode provides reasonable PCE, reaching 55.2% PCE of that obtained using ITO anode.

The possibility of utilizing graphene film as hole-collecting materials was explored recently.<sup>75</sup> Eda et al.<sup>75</sup> reported the preparation of transparent and

conductive graphene film achieved by vacuum filtering graphite oxide to form a film followed by hydrazine vapor reduction and low temperature annealing under nitrogen to reduce film resistance. They found that film treatment with SOCl<sub>2</sub> could reduce the film resistance by five times. The obtained graphene film was then incorporated into organic solar cells using PEDOT:PSS, poly(3-hexylthiophene) (P3HT) and phenyl-C61-butyric acid methyl ester (PCBM) as active material and aluminum as top electrode. The PCE of the fabricated cells was ~0.1%. The results from the reference experiment excluding graphene film in solar cell indicated that the reduced graphite oxide film (instead of PEDOT:PSS) acted as hole collecting electrode in the cell. Very recently, Yun et al.<sup>76</sup> investigated the solution-processable reduced graphene oxide thin films as a novel alternative to PEDOT:PSS hole transport anode interfacial layer for fabricating highly efficient and stable polymer solar cells. The efficiency of the cells reached 3.63% and showed a much longer cell lifetime in air stability tests in comparison with PEDOT:PSS-based cells (Figure 9).

Dye-sensitized solar cells have attracted considerable attention due to their low production cost and

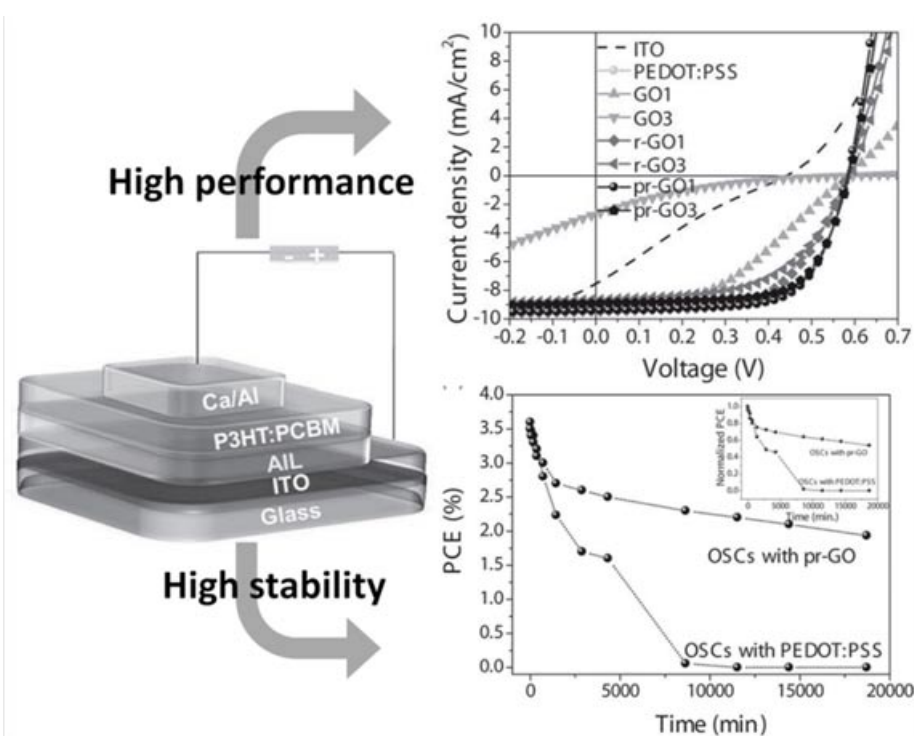


**FIGURE 9** | The preparation of newly reduced graphene oxide (pr-GO) was with a novel *p*-TosNHNH<sub>2</sub> reductant. The pr-GO was used as an efficient anode interfacial layer for high-performance and high-stability OSCs. The efficiency of the cells with pr-GO (3.63%) was highly comparable to those of the PEDOT:PSS-based devices. Furthermore, the pr-GO-based organic solar cells showed a much longer cell lifetime in air stability tests in comparison with PEDOT:PSS-based cells. (Reprinted with permission from Ref 76. Copyright 2011, John Wiley and Sons, Ltd.)

relatively high energy conversion efficiency. In this device, counter electrode is an indispensable component, which catalyzes the reduction of  $I_2$  to  $I^-$  after electron injection. As most commonly used Pt catalytic material is quite expensive, developing low-cost alternative materials is necessary and attractive. Recently, Shi and co-workers<sup>77</sup> reported a novel counter electrode for solar cell on which the 1-pyrenebutyrate functionalized graphene was incorporated into FTO (G-FTO) to form the composite electrode. The PCE (2.2%) of the cell utilizing G-FTO as counter electrode was significantly higher than that (0.048%) of the cell using FTO as counter electrode yet still inferior with respect to the cell using platinum as counter electrode (3.98%). Accounting the fact that PEDOT:PSS shows good transparency and moderate conductance as counter electrode, graphene doping of PEDOT:PSS has also been performed.<sup>78</sup> The cell using graphene/PEDOT:PSS as counter electrode showed a PCE of 4.5% which was comparable to that from cells using Pt as counter electrode (6.3%) and even higher than that of cells using PEDOT:PSS as counter electrode (2.3%).

Heterojunction solar cells are devices that convert solar energy to electrical power via photovoltaic effect of p-n junctions. On the basis of its superior electrical property, graphene has been studied for applications in heterojunction solar cells during the past several years. Most studies focused on  $C_{60}$  derivatives as electron acceptors of polymer-based organic photovoltaics (OPV). For example, graphene was functionalized by phenyl isocyanate or butylamine to provide high solubility prior to blending with poly(3-hexylthiophene) (P3HT) or poly(3-octylthiophene) (P3OT).<sup>79,80</sup> The synthesized P3OT/graphene solar cell showed 0.32% power conversion efficiency. After annealing, however, the efficiency increased to 1.4% due to the removal of functional groups from the graphene component as well as the improved morphology and crystallinity of the P3OT component.<sup>79</sup> The graphene/P3HT solar cell also showed a similar efficiency of 1.1%.<sup>81,82</sup> Although this value is considered lower than the state-of-the-art OPVs (probably due to the irregular molecular structure of the reduced graphene oxide), it is substantially better than those showed by the CNT-based cells. Furthermore, a theoretical study predicts that the graphene-based OPV may provide efficiency in excess of 12% in a single cell; thus, it is strongly expected that further optimization might give a breakthrough from the current OPVs limitation.<sup>83</sup> Moreover, employing a similar structure to that of heterojunction cells, a Schottky junction solar cell based on graphene/n-silicon was constructed.<sup>84</sup> By transferring a

graphene film directly onto a pretreated n-type silicon/ $SiO_2$  wafer, a solar cell featuring an energy conversion efficiency of 1.65% was demonstrated. Other two kind of Schottky junction solar cells were also assembled by directly coating graphene films on n-type silicon nanowire (SiNW) arrays<sup>85</sup> or CdSe nanobelt.<sup>86</sup> The graphene/SiNW-based solar cells provide energy conversion efficiencies up to 2.86%.<sup>85</sup>

In summary, graphene has also emerged as one of the core nanomaterials for solar cells application, especially as an alternative of the conventional electrode materials. Currently, the relatively low PCE of the cell seems to be closely related with the high resistance of the graphene films. Further research efforts on this aspect as well as on the electron-transfer behavior of the graphene film is thus warranted.

## APPLICATIONS OF GRAPHENE IN FUEL CELLS

Fuel cell is an energy conversion device, which produces energy by oxidizing a fuel catalyzed by the catalysts immobilized on electrodes.<sup>87</sup> Low-temperature fuel cell works below 200°C and electrochemically converts hydrogen into water or methanol-ethanol into water and carbon dioxide.<sup>88</sup> The fuel cell performance is also mainly determined by their electrodes, particularly cathode. Platinum and its alloys are currently the most efficient electrocatalysts in cathode for oxygen reduction reaction (ORR). Here, the high price of platinum limits its practical applications. Immobilizing Pt nanoparticles on a substrate with high specific surface area has become the most widely used technique to improve the activity and efficiency of Pt catalyst. Graphene is the ideal catalyst support considering its high electrical conductivity, robust mechanical properties, high specific surface area, unique graphitic basal plane structure, and low cost.

Liu et al. compared the specific surface area, electrocatalytic activity for ORR and stability of Pt nanoparticles supported on the functionalized graphene sheets (FGS) and carbon blacks (E-TEK) under the same testing conditions.<sup>89</sup> Pt-FGS provides not only larger surface area and higher ORR activity (relative to Pt-E-TEK) but also stable performance during 5000 cyclic voltammetry cycles. These improved properties were attributed to the reduced aggregation of Pt particles immobilized on graphene. Pt nanoparticles were also supported on graphene nanoplatelets on which a good electrochemical durability (two to three times that of the Pt/CNT or E-TEK Pt/C) was attained.<sup>90</sup>

The morphology and the dispersion of Pt nanoparticles highly influence their catalytic

activities. Layer-by-layer (LBL) self-assembly is considered as an effective approach to adjust material's structures on nanometer scale.<sup>91</sup> An imidazolium salt-based ionic liquid functionalized graphene and platinum nanoparticles were LBL assembled into a three-dimensional hybrid nanostructure. Pt nanoparticles were uniformly dispersed on the surfaces of graphene sheets and the resultant composite showed high electrocatalytic activity. The electrocatalytic activity of the composite can also be adjusted as a function of its bilayer number. Liu et al.<sup>92</sup> reported a green electrochemical approach to produce Pt/graphene composites. Pt nanoparticles were uniformly deposited on graphene sheets. The ORR current density at the composite electrode was much higher than that obtained using a Pt nanoparticle-modified glassy carbon electrode. Furthermore, the onset potential of the ORR for the former electrode was substantially higher than that for the latter electrode. Nitrogen-doped carbon material has also been claimed as a good support for Pt catalyst. The doped nitrogen atoms act as the anchoring sites for the metal particles and chemically active sites for catalytic reactions.<sup>93</sup> Jafri et al.<sup>94</sup> utilized GNSs and nitrogen-doped GNSs as the electrocatalyst support for Pt nanoparticles in PEMFCs. The constructed fuel cells provided power densities of 440 and 390  $\text{mW cm}^{-2}$  when nitrogen-doped GNS–Pt and GNS–Pt was used, respectively. Nitrogen doping process creates pyrrolic nitrogen defects, which act as anchoring sites for Pt nanoparticles and might be responsible for the increased electrical conductivity and/or improved carbon-catalyst binding. The introduction of carbon might also increase the electron mobility of the catalyst support. Recently, the dispersion of Pt on graphene oxide was shown to be crucial toward achieving enhanced fuel cell performance, as

shown in Figure 10. Here, using graphene oxide as a support material to distribute Pt nanoparticles provides a new method to obtain advanced electrocatalyst materials for hydrogen-based fuel cells. A partially reduced graphene oxide–Pt-based fuel cell delivered a maximum power of 161  $\text{mW cm}^{-2}$  relative to 96  $\text{mW cm}^{-2}$  achieved for an unsupported Pt-based fuel cell.<sup>95</sup>

A great deal of efforts has been devoted to find low-cost alternative materials with high catalytic activities to replace Pt. Among them, nitrogen-doped carbon materials such as nitrogen-doped CNTs or graphene are promising. Numerous metal free materials were also screened as the fuel cell catalysts. Nitrogen-doped carbon materials (e.g., CNTs, graphene) and graphitic carbon nitride were claimed as good catalysts for ORR.<sup>90,96–99</sup> Nitrogen-doped graphene can be synthesized by chemical vapor deposition of methane in the presence of ammonia.<sup>99</sup> Compared to Pt, this material demonstrated higher electrocatalytic activity, better stability, and improved tolerance toward CO. Its low price and high electrocatalytic activity justifies nitrogen-doped graphene (shown in Figure 11a) use for fuel cells electrocatalyst. The electrocatalytic mechanism of nitrogen-doped graphene in acidic environment has been studied by Zhang et al.<sup>100</sup> using density functional theory (DFT) showed in Figure 11(b). Their simulation suggests that the ORR on nitrogen-doped graphene takes place according to a direct four-electron pathway, which is consistent with the experimental observations. The energy calculated for each ORR step verifies that the ORR can spontaneously occur on the N-graphene. The active catalytic sites on single nitrogen-doped graphene are identified as well, which have either high positive spin density or high

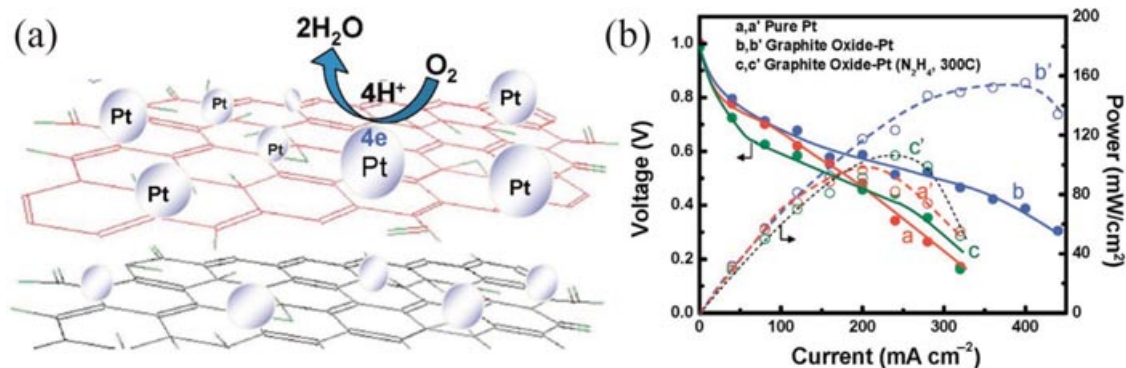


**FIGURE 10** | (a) Scheme shows dispersion of Pt nanoparticles on a two-dimensional carbon sheet (graphene) to facilitate an electrocatalytic reaction. (b) Galvanostatic fuel cell polarization (I–V) curves (a–c) and power characteristics (a'–c'). The cathode was composed of (a, a') Pt, (b, b') GO–Pt, and GO–Pt (hydrazine, 300°C treated). The partially reduced GO–Pt-based fuel cell delivered a maximum power of 161  $\text{mW cm}^{-2}$  compared to 96  $\text{mW cm}^{-2}$  for an unsupported Pt-based fuel cell. (Reprinted with permission from Ref 95. Copyright 2009, American Chemical Society.)

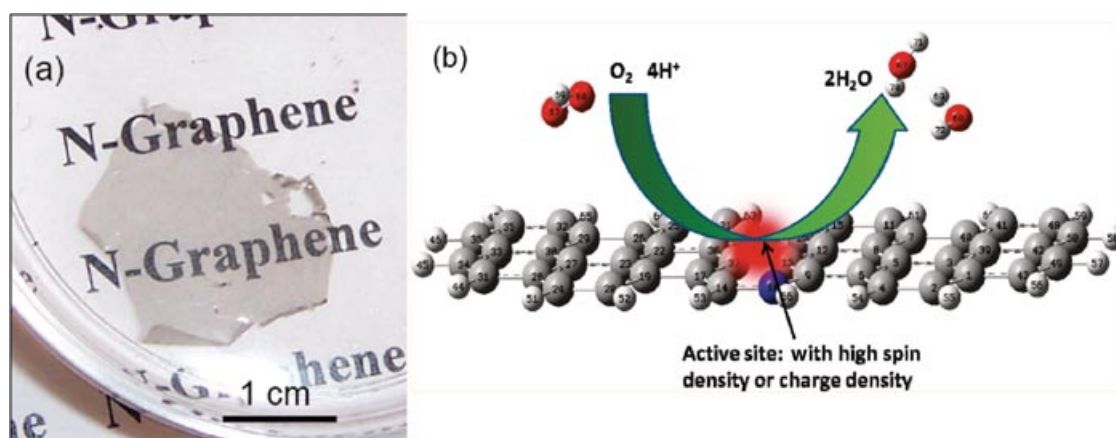


**FIGURE 11** | (a) Digital photo image of transparent nitrogen-doped graphene film floating on water after removal of the nickel layer by dissolving in an aqueous acid solution. (b) The electrocatalytic mechanism of nitrogen-doped graphene in acidic environment. (Reprinted with permission from Refs 99 and 100. Copyright 2010 and 2011, American Chemical Society.)

positive atomic charge density. The nitrogen doping introduces asymmetric spin density and atomic charge density, making high electrocatalytic activities in N-graphene feasible. Another study on nitrogen-doped graphene electrocatalyst was performed by Shao and co-workers.<sup>90</sup> In this study, they synthesized the material by exposing graphene to nitrogen plasma.

Another fuel cell type, direct methanol fuel cells (DMFC) have drawn great attention in terms of their high energy density, zero emission, ease fuel (methanol) handling and storage in low operating temperatures (60–100°C). Again, low electrocatalytic activity for methanol oxidation and safety issues re-

lated to methanol toxicity hinders its commercialization. In this device, graphene might also be exploited as electrocatalysts. Recent studies demonstrated that the platinum/graphene (Pt/GNS) catalyst shows a high catalytic activity for both methanol oxidation and ORRs.<sup>101–103</sup> Ajayan et al.<sup>101</sup> investigated the deposition of Pt nanoparticles onto surfaces of GO nanosheets with particle size in the range of 1–5 nm by ethylene glycol reduction. During Pt deposition, a majority of oxygenated functional groups on GO was removed, which resulted in a Pt/CCG hybrid. The electrochemically active surface areas of Pt/CCG and a comparative sample of Pt/CNTs are 36.27

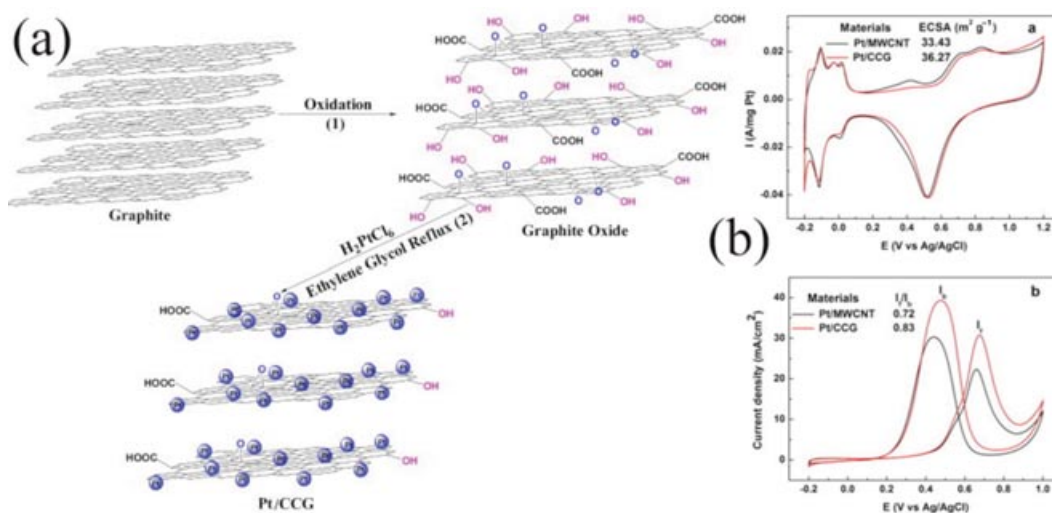


**FIGURE 12** | (a) Scheme shows a formation route to anchor Pt nanoparticles onto chemically converted graphene (CCG) nanosheets. (1) Oxidation of pure graphite powder to graphite oxide. (2) Formation of Pt/CCG hybrids. (b) Electrochemical catalytic performances of Pt/CCG and Pt/MWCNT hybrids. The electrochemically active surface areas measured from (a) for Pt/CCG and Pt/MWCNT are 36.27 and 33.43 m<sup>2</sup> g<sup>-1</sup>, respectively. The  $I_a/I_b$  ratios measured from (b) for Pt/CCG and Pt/MWCNT are 0.83 and 0.72, respectively. (Reprinted with permission from Ref 101. Copyright 2010, Elsevier.)

and  $33.43 \text{ m}^2 \text{ g}^{-1}$ , respectively. The Pt/CCG hybrid shows better tolerance to CO for electro-oxidation of methanol compared to the Pt/MWCNT catalyst (Figure 12). Xin et al.<sup>102</sup> deposited Pt nanoparticles onto GNS via synchronous reduction of  $\text{H}_2\text{PtCl}_6$  and GO suspension using  $\text{NaBH}_4$ . The current density of Pt/GNS catalyst ( $182.6 \text{ mA mg}^{-1}$ ) outperforms that of Pt/C catalyst ( $77.9 \text{ mA mg}^{-1}$ ). Moreover, the application of heat treatment on the Pt/GNS catalyst improved the performance further by  $\sim 3.5$  times over that of the Pt/C catalyst. Similarly, Li and co-workers<sup>103</sup> prepared the composites of graphene and Pt nanoclusters via reduction of graphite oxide and  $\text{H}_2\text{PtCl}_6$ . Methanol oxidation results indicated that Pt/GNS had better catalytic performance with respect to Pt/Vulcan catalyst. The peak current of Pt/GNS was nearly twice that of the conventional Pt/Vulcan catalysts. The stability of Pt/GNS was also better relative to Pt/Vulcan catalyst. Other work reported that improved catalytic activity toward methanol oxidation in DMFC can be obtained by using a GNS supported Pt–Ruthenium (Pt–Ru) nanocomposite or Pt–Ru dispersed graphene-functionalized multiwalled carbon nanotubes (Pt–Ru/(f–Gef–MWNT)) instead of a Pt–Ru/Vulcan, Pt–Ru/f–MWNT or Pt–Ru/f–G.<sup>104,105</sup> Dong et al.<sup>106</sup> has also demonstrated that Pt and Pt–Ru nanoparticles synthesized onto GNSs exhibit high electrocatalytic activity toward methanol and ethanol, leading to a greatly reduced overpotential and increased reversibility. These findings favor the use of graphene sheets as catalyst supports in direct methanol and ethanol fuel cells. Moreover, Shang et al.<sup>107</sup> investigated the application of uniform and porous GNSs as a support for catalytic Pt nanoclusters in direct-methanol electro-oxidation. They noted that composite materials exhibit superior electrochemical characteristics than the each component by itself.

## CONCLUSIONS

Energy conversion and storage devices utilizing renewable resources with zero emission are the key technology toward sustainable future development of our society, keeping in mind the constantly increasing energy demand and environmental compatibility requirements. Graphene, a relatively new carbon nanomaterial endowed with unique structural and electro-

chemical properties, has found its application in all sorts of energy related devices such as supercapacitors, batteries, solar cells, and fuel cells. This paper overviews some of the recent substantial progresses on the performance and status of these graphene-based devices. The excellent electron-transfer properties as well as the unique two-dimensional structure of the graphene have favored its usage as electrode in these devices. In particular, graphene films with good transparency, high conductance, and proper work function stands as a promising alternative electrode candidate to replace ITO and FTO for solar cells and other optoelectronics applications. Graphene serves as a good support material for Pt catalyst in fuel cell applications considering its high catalytic activity and specific surface area. Graphene-based electrode materials also display excellent capacitance and good cycling performance in RLBs. The encapsulation of metal or metal oxide nanoparticles with graphene can improve the cycling performance of these anode materials in RLBs applications. Moreover, graphene materials featuring mesoporous structures in combination with large accessible surface area demonstrates superior capacitance in EDLCs applications. The incorporation of graphene into the electrode of EDLC seems to contribute positively toward the power density performance.

However, research on the application of graphene and graphene-based materials in clean energy supply and storage devices is still at a premature stage. A number of challenges remain to be explored, such as precise tuning of the function and the property of the structures; economic, scalable, and green production of the materials; and efficient integration of materials into high-performance devices. Besides experimental studies, theoretical investigations of graphene and graphene-based nanostructures on various aspects, such as charge and electron transport behaviors, edge, defects, doping effects, phase to phase interactions, and so on, are essential as well for understanding deeper the structure–property relationship of the materials and reasonable designing of novel nanostructures and devices associated with graphene. Nevertheless, graphene and graphene-based nanomaterials have emerged as highly attractive components in energy related devices, and will play an important role in the future for the development of clean energy technologies.

## ACKNOWLEDGMENTS

Financial supported from the National Natural Science Foundation of China (20973044, 21173057), the Ministry of Science and Technology of China (2009AA03Z328,

2009DPA41220, 2012CB933402), the Chinese Academy of Sciences (KJCX2-YW-H21), and the Guangdong-CAS strategic cooperation Program (2009B091300007) is acknowledged.

## REFERENCES

1. Conibeer G. Third-generation photovoltaics. *Mater Today* 2007, 11:42–50.
2. Winter M, Besenhard JO, Spahr ME, Novák P. Insertion electrode materials for rechargeable lithium batteries. *Adv Mater* 1998, 10:725–763.
3. Simon P, Gogotisi Y. Materials for electrochemical capacitors. *Nat Mater* 2008, 7:845–854.
4. Gratzel M. Dye-sensitized solar cells. *J Photochem Photobiol C* 2003, 4:145–153.
5. Coelho B, Oliveira AC, Mendes A. Concentrated solar power for renewable electricity and hydrogen production from water—a review. *Energy Environ Sci* 2010, 3:1398–1405.
6. Winter M, Brodd RJ. What are batteries, fuel cells, and supercapacitors? *Chem Rev* 2004, 104:4245–4269.
7. Arico AS, Bruce P, Scrosati B, Tarascon JM, Schalkwijk WV. Nanostructured materials for advanced energy conversion and storage devices. *Nat Mater* 2005, 4:366–377.
8. Spanggaard H, Krebs FC. A brief history of the development of organic and polymeric photovoltaics. *Sol Energy Mater Sol Cells* 2004, 83:125–146.
9. Hall PJ, Mirzaei M, Fletcher SI, Sillars FB, Rennie AJR, Shitta-Bey GO, Wilson G, Cruden A, Carter R. Energy storage in electrochemical capacitors: designing functional materials to improve performance. *Energy Environ Sci* 2010, 3:1238–1251.
10. Liu C, Li F, Ma LP, Cheng HM. Advanced materials for energy storage. *Adv Mater* 2010, 22:E28–E62.
11. Novoselov KS, Geim AK, Morozov SV, Jiang D, Zhang Y, Dubonos SV, Grigorieva IV, Firsov AA. Electric field effect in atomically thin carbon films. *Science* 2004, 306:666–669.
12. Zhang YB, Tan YW, Stormer HL, Kim P. Experimental observation of the quantum Hall effect and Berry's phase in graphene. *Nat Mater* 2005, 4:38:201–204.
13. Falkovsky LA. Optical properties of graphene and IV–VI semiconductors. *Phys-Usp* 2008, 51:887–897.
14. Foster MS, Aleiner IL. Slow imbalance relaxation and thermoelectric transport in graphene. *Phys Rev B* 2009, 79:085415.
15. Geim AK, Novoselov KS. The rise of graphene. *Nat Mater* 2007, 6:183–191.
16. Chen D, Tang LH, Li JH. Graphene-based materials in electrochemistry. *Chem Soc Rev* 2010, 39:3157–3180.
17. Pumera M. Electrochemistry of graphene: new horizons for sensing and energy storage. *Chem Rec* 2009, 9:211–223.
18. Brownson DAC, Banks CE. Graphene electrochemistry: an overview of potential applications. *Analyst* 2010, 135:2768–2778.
19. Liang MH, Zhi LJ. Graphene-based electrode materials for rechargeable lithium batteries. *J Mater Chem* 2009, 19:5871–5878.
20. Scheuermann GM, Rumi L, Steurer P, Bannwarth W, Mulhaupt R. Palladium nanoparticles on graphite oxide and its functionalized graphene derivatives as highly active catalysts for the Suzuki–Miyaura coupling reaction. *J Am Chem Soc* 2009, 131:8262–8270.
21. Robinson JT, Perkins FK, Snow ES, Wei ZQ, Sheehan PE. Reduced graphene oxide molecular sensors. *Nano Lett* 2008, 8:3137–3140.
22. Park S, Mohanty N, Suk JW, Nagaraja A, An JH, Piner RD, Cai WW, Dreyer DR, Berry V, Ruoff RS. Biocompatible, robust free-standing paper composed of a tween/graphene composite. *Adv Mater* 2010, 22:1736–1740.
23. Hu YH, Wang H, Hu B. Thinnest two-dimensional nanomaterial-graphene for solar energy. *ChemSusChem* 2010, 3:782–796.
24. Liang MH, Luo B, Zhi LJ. Application of graphene and graphene-based materials in clean energy-related devices. *Int J Energy Res* 2009, 33:1161–1170.
25. Simon P, Gogotisi Y. Materials for electrochemical capacitors. *Nat Mater* 2008, 7:845–854.
26. Barbieri O, Hahn M, Herzog A, Kotz R. Capacitance limits of high surface area activated carbons for double layer capacitors. *Carbon* 2005, 43:1303–1310.
27. Stoller MD, Park SJ, Zhu YW, An J, Ruoff RS. Graphene-based ultracapacitors. *Nano Lett* 2008, 8:3498–3502.
28. Zhu YW, Murali S, Stoller MD, Velamakanni A, Piner RD, Ruoff RS. Microwave assisted exfoliation and reduction of graphite oxide for ultracapacitors. *Carbon* 2010, 48:2106–2122.
29. Zhu YW, Murali S, Stoller MD, Ganesh KJ, Cai WW, Ferreira PJ, Pirkle A, Wallace RM, Cychosz KA, Thommes M, et al. Carbon-based supercapacitors produced by activation of graphene. *Science* 2011, 332:1537–1541.
30. Ning GQ, Fan ZJ, Wang G, Gao JS, Qian QZ, Wei F. Gram-scale synthesis of nanomesh graphene with high surface area and its application in supercapacitor electrodes. *Chem Commun* 2011, 47:5976–5978.

31. Miller JR, Outlaw RA, Holloway BC. Graphene double-layer capacitor with ac line-filtering performance. *Science* 2010, 329:1637–1639.
32. Yoo JJ, Balakrishnan K, Huang JS, Meunier V, Sumpter BG, Srivastava A, Conway M, Reddy ALM, Yu J, Vajtai R, et al. Ultrathin planar graphene supercapacitors. *Nano Lett* 2011, 11:1423–1427.
33. Liu CG, Yu ZN, Neff D, Zhamu A, Jang BZ. Graphene-based supercapacitor with an ultrahigh energy density. *Nano Lett* 2010, 10:4863–4868.
34. Shao JJ, Wu SD, Zhang SB, Lv W, Su FY, Yang QH. Graphene oxide hydrogel at solid/liquid interface. *Chem Commun* 2011, 47:5771–5773.
35. Xu YX, Sheng KX, Li C, Shi GQ. Self-assembled graphene hydrogel via a one-step hydrothermal process. *ACS Nano* 2010, 4:4324–4330.
36. Zhang L, Shi GQ. Preparation of highly conductive graphene hydrogels for fabricating supercapacitors with high rate capability. *J Phys Chem C* 2011, 115:17206–17212.
37. Wu Q, Sun YQ, Bai H, Shi GQ. High-performance supercapacitor electrodes based on graphene hydrogels modified with 2-aminoanthraquinone moieties. *Phys Chem Chem Phys* 2011, 13:11193–11198.
38. Fan ZJ, Yan J, Zhi LJ, Zhang Q, Wei T, Feng J, Zhang ML, Qian WZ, Wei F. A three-dimensional carbon nanotube/graphene sandwich and its application as electrode in supercapacitors. *Adv Mater* 2010, 22:3723–3728.
39. Lei ZB, Christov N, Zhao XS. Intercalation of mesoporous carbon spheres between reduced graphene oxide sheets for preparing high-rate supercapacitor electrodes. *Energy Environ Sci* 2011, 4:1866–1873.
40. Jeong HM, Lee JW, Shin WH, Choi YJ, Shin HJ, Kang JK, Choi JW. Nitrogen-doped graphene for high-performance ultracapacitors and the importance of nitrogen-doped sites at basal planes. *Nano Lett* 2011, 11:2472–2477.
41. Wu ZS, Wang DW, Ren WC, Zhao JP, Zhou GM, Li F, Cheng HM. Anchoring hydrous RuO<sub>2</sub> on graphene sheets for high-performance electrochemical capacitors. *Adv Funct Mater* 2010, 20:3595–3602.
42. Lv W, Sun F, Tang DM, Fang HT, Liu C, Yang QH, Cheng HM. A sandwich structure of graphene and nickel oxide with excellent supercapacitive performance. *J Mater Chem* 2011, 21:9014–9019.
43. Fan ZJ, Yan J, Wei T, Zhi LJ, Ning GQ, Li TY, Wei F. Asymmetric supercapacitors based on graphene/MnO<sub>2</sub> and activated carbon nanofiber electrodes with high power and energy density. *Adv Funct Mater* 2011, 21:2366–2375.
44. Yu GH, Hu LB, Vosgueritchian M, Wang HL, Xie X, McDonough JR, Cui X, Cui Y, Bao ZN. Solution-processed graphene/MnO<sub>2</sub> nanostructured textiles for high-performance electrochemical capacitors. *Nano Lett* 2011, 11:2905–2911.
45. Kang K, Meng YS, Breger J, Grey CP, Ceder G. Electrodes with high power and high capacity for rechargeable lithium batteries. *Science* 2006, 311:977–980.
46. Kim MG, Cho J. Reversible and high-capacity nanostructured electrode materials for Li-ion batteries. *Adv Funct Mater* 2009, 19:1497–1514.
47. Wang GX, Shen XP, Yao J, Park J. Graphene nanosheets for enhanced lithium storage in lithium ion batteries. *Carbon* 2009, 47:2049–2053.
48. Dahn JR, Zheng T, Liu YH, Xue JS. Mechanism for lithium insertion in carbonaceous materials. *Science* 1995, 270:590–593.
49. Liu YH, Xue JS, Zheng T, Dahn JR. Mechanism of lithium insertion in hard carbons prepared by pyrolysis of epoxy resins. *Carbon* 1996, 34:193–200.
50. Kumar A, Reddy ALM, Mukherjee A, Dubey M, Zhan XB, Singh N, Ci LJ, Billups WE, Nagurny J, Mital G, et al. Direct synthesis of lithium-intercalated graphene for electrochemical energy storage application. *ACS Nano* 2011, 5:4345–4349.
51. Yoo EJ, Kim J, Hosono E, Zhou HS, Kudo T, Honma I. Large reversible Li storage of graphene nanosheet families for use in rechargeable lithium ion batteries. *Nano Lett* 2008, 8:2277–2282.
52. Yang SB, Feng XL, Zhi LJ, Cao Q, Maier J, Mullen K. Nanographene-constructed hollow carbon spheres and their favorable electroactivity with respect to lithium storage. *Adv Mater* 2010, 22:838–842.
53. Wu ZS, Ren WC, Xu L, Li F, Cheng HM. Doped graphene sheets as anode materials with superhigh rate and large capacity for lithium ion batteries. *ACS Nano* 2011, 5:5463–5471.
54. Paek SM, Yoo EJ, Honma I. Enhanced cyclic performance and lithium storage capacity of SnO<sub>2</sub>/Graphene nanoporous electrodes with three-dimensionally delaminated flexible structure. *Nano Lett* 2009, 9:72–75.
55. Lee KT, Jung YS, Oh SM. Synthesis of tin-encapsulated spherical hollow carbon for anode material in lithium secondary batteries. *J Am Chem Soc* 2003, 125:5652–5653.
56. Cui GL, Hu YS, Zhi LJ, Wu DQ, Lieberwirth I, Maier J, Mullen K. A one-step approach towards carbon-encapsulated hollow tin nanoparticles and their application in lithium batteries. *Small* 2007, 3:2066–2069.
57. Zhang WM, Wu XL, Hu JS, Guo YG, Wan LJ. Carbon coated Fe<sub>3</sub>O<sub>4</sub> nanospindles as a superior anode material for lithium-ion batteries. *Adv Funct Mater* 2008, 18:3941–3946.
58. Yang SB, Feng XL, Ivanovici S, Mullen K. Fabrication of graphene-encapsulated oxide nanoparticles: towards high-performance anode materials for lithium storage. *Angew Chem Int Ed* 2010, 49:8408–8411.

59. Wang HL, Cui LF, Yang Y, Casalongue S, Robinson JT, Liang YY, Cui Y, Dai HJ.  $Mn_3O_4$  graphene hybrid as a high-capacity anode material for lithium ion batteries. *J Am Chem Soc* 2010, 132:13978–13980.
60. Ding Y, Jiang Y, Xu F, Yin J, Ren H, Zhuo Q, Long Z, Zhang P. Preparation of nano-structured  $LiFePO_4$ /graphene composites by co-precipitation method. *Electrochem Commun* 2010, 12:10–13.
61. Wang HL, Yang Y, Liang YY, Robinson JT, Li YG, Jackson A, Cui Y, Dai HJ. Graphene-wrapped sulfur particles as a rechargeable lithium-sulfur battery cathode material with high capacity and cycling stability. *Nano Lett* 2011, 11:2644–2647.
62. Ellis BL, Lee KT, Nazar LF. Positive electrode materials for Li-ion and Li-batteries. *Chem Mater* 2010, 22, 691–714.
63. Wang J, Lu L, Choucair M, Stride JA, Xu X, Liu H. Sulfur-graphene composite for rechargeable lithium batteries. *J Power Sources* 2011, 196:7030–7034.
64. Bonaccorso F, Sun Z, Hasan T, Ferrari AC. Graphene photonics and optoelectronics. *Nat Photonics* 2010, 4:611–622.
65. Eda G, Chhowalla M. Chemically derived graphene oxide: towards large-area thin-film electronics and optoelectronics. *Adv Mater* 2010, 22:2392–2415.
66. Wassei JK, Kaner RB. Graphene, a promising transparent conductor. *Mater Today* 2010, 13:52–59.
67. Schmidt-Mende L, Fechtenkötter A, Müllen K, Moons E, Friend RH, MacKenzie JD. Self-organized discotic liquid crystals for high-efficiency organic photovoltaics. *Science* 2001, 293:1119–1122.
68. Wang X, Zhi LJ, Mullen K. Transparent, conductive graphene electrodes for dye-sensitized solar cells. *Nano Lett* 2008, 8:323–327.
69. Wang X, Zhi LJ, Tsao N, Tomovic Z, Li JL, Mullen K. Transparent carbon films as electrodes in organic solar cells. *Angew Chem. Int Ed* 2008, 47:2990–2992.
70. Becerril HA, Mao J, Liu Z, Stoltenberg RM, Bao Z, Chen Y. Evaluation of solution-processed reduced graphene oxide films as transparent conductors. *Acc Nano* 2008, 2:463–470.
71. Stankovich S, Dikin DA, Dommett GHB, Kohlhaas KM, Zimney EJ, Stach EA, Piner RD, Nguyen ST, Ruoff RS. Graphene-based composite materials. *Nature* 2006, 442:282–286.
72. Watcharotone S, Dikin DA, Stankovich S, Piner R, Jung I, Dommett GHB, Evmenenko G, Wu SE, Chen SF, Liu CP, et al. Graphene-silica composite thin films as transparent conductors. *Nano Lett* 2007, 7:1888–1892.
73. Wu SE, Chen SF, Liu CP, Nguyen ST, Ruoff RS. Graphene-silica composite thin films as transparent conductors. *Nano Lett* 2007, 7:1888–1892.
74. Wang Y, Chen XH, Zhong YL, Zhu FR, Loh KP. Large area, continuous, few-layered graphene as anodes in organic photovoltaic devices. *Appl Phys Lett* 2009, 95:063302–063303.
75. Eda G, Lin YY, Miller S, Chen CW, Su WF, Chhowalla M. Transparent and conducting electrodes for organic electronics from reduced graphene oxide. *Appl Phys Lett* 2008, 93:233305.
76. Yun JM, Yei JS, Kim J, Jeong HG, Kim DY, Noh YJ, Kim SS, Ku BC, Na SI. Solution-Processable Reduced Graphene Oxide as a Novel Alternative to PEDOT:PSS Hole Transport Layers for Highly Efficient and Stable Polymer Solar Cells. *Adv Mater* 2011, 23:4923–4928.
77. Xu Y, Bai H, Lu G, Li C, Shi GQ. Flexible graphene films via the filtration of water-soluble noncovalent functionalized graphene sheets. *J Am Chem Soc* 2008, 130:5856–5857.
78. Hong WJ, Xu YX, Lu GW, Li C, Shi GQ. Transparent graphene/PEDOT-PSS composite films as counter electrodes of dye-sensitized solar cells. *Electrochem Commun* 2008, 10:1555–1558.
79. Liu ZF, Liu Q, Huang Y, Ma YF, Yin SG, Zhang XY, Sun W, Chen Y. Organic photovoltaic devices based on a novel acceptor material: graphene. *Adv Mater* 2008, 20:3924–3930.
80. Valentini L, Cardinali M, Bon SB, Bagnis D, Verdejo R, Lopez-Manchado MA, Kenny JM. Use of butylamine modified graphene sheets in polymer solar cells. *J Mater Chem* 2010, 20:995–1000.
81. Liu Q, Liu ZF, Zhang XY, Zhang N, Yang LY, Yin SG, Chen YS. Organic photovoltaic cells based on an acceptor of soluble graphen. *Appl Phys Lett* 2008, 92:223303.
82. Liu Q, Liu ZF, Zhang XY, Zhang N, Yang LY, Zhang N, Pan G, Yin SG, Chen YS, Wei J. Polymer photovoltaic cells based on solution-processable graphene and P3HT. *Adv Funct Mater* 2009, 19:894–904.
83. Yong V, Tour JM. Theoretical efficiency of nanostructured graphene-based photovoltaics. *Small* 2010, 6:313–318.
84. Li XM, Zhu HW, Wang KL, Cao AY, Wei JQ, Li CY, Jia Y, Li Z, Li X, Wu DH. Graphene-on-silicon Schottky junction solar cells. *Adv Mater* 2010, 22, 2743–2748.
85. Fan GF, Zhu HW, Wang KL, Wei JQ, Li XM, et al. Graphene/silicon nanowire Schottky junction for enhanced light harvesting. *ACS Appl Mater Interfaces* 2011, 3:721–725.
86. Zhang LH, Fan LL, Li Z, Shi EZ, Li XM, Li HB, Ji CY, Jia Y, Wei JQ, Wang K. Graphene-CdSe nanobelt solar cells with tunable configurations. *Nano Res* 2011, 4:891–900.
87. Antolini E. Catalysts for direct ethanol fuel cells. *J Power Sources* 2007, 170:1–12.

88. Antolini E. Carbon supports for low-temperature fuel cell catalysts. *Appl Catal B* 2009, 88:1–24.
89. Kou R, Shao YY, Wang DH, Engelhard MH, Kwak JH, Wang J, Viswanathana VV, Wang CM, Lin YH, Wang Y, et al. Enhanced activity and stability of Pt catalysts on functionalized graphene sheets for electrocatalytic oxygen reduction. *Electrochem Commun* 2009, 11:954–957.
90. Shao YY, Zhang S, Wang CM, Nie ZM, Liu J, Wang Y, Lin YH. Highly durable graphene nanoplatelets supported Pt nanocatalysts for oxygen reduction. *J Power Sources* 2010, 195:4600–4605.
91. Zhu CZ, Guo SJ, Zhai YM, Dong SJ. Layer-by-layer self-assembly for constructing a graphene/platinum nanoparticle three-dimensional hybrid nanostructure using ionic liquid as a linker. *Langmuir* 2010, 26:7614–7618.
92. Liu S, Wang JQ, Zeng J, Ou JF, Li ZP, Liu XH, Yang SR. “Green” electrochemical synthesis of Pt/graphene sheet nanocomposite film and its electrocatalytic property. *J Power Sources* 2010, 195:4628–4633.
93. Zhang LS, Liang XQ, Song WG, Wu ZY. Identification of the nitrogen species on N-doped graphene layers and Pt/NG composite catalyst for direct methanol fuel cell. *Phys Chem Chem Phys* 2010, 12:12055–12059.
94. Jafri RI, Rajalakshmi N, Ramaprabhu S. Nitrogen doped graphene nanoplatelets as catalyst support for oxygen reduction reaction in proton exchange membrane fuel cell. *J Mater Chem* 2010, 20:7114–7117.
95. Seger B, Kamat PV. Electrocatalytically active graphene-platinum nanocomposites. role of 2-D carbon support in PEM fuel cells. *J Phys Chem C* 2009 113:7990–7995.
96. Sun YQ, Li C, Xu YX, Bai H, Yao ZY, Shi GQ. Chemically converted graphene as substrate for immobilizing and enhancing the activity of a polymeric catalyst. *Chem Commun* 2010, 46:4740–4742.
97. Gong KP, Du F, Xia ZH, Durstock M, Dai LM. Nitrogen-doped carbon nanotube arrays with high electrocatalytic activity for oxygen reduction. *Science* 2009, 323:760–764.
98. Tang YF, Allen BL, Kauffman DR, Star A. Electrocatalytic activity of nitrogen-doped carbon nanotube cups. *J Am Chem Soc* 2009, 131:13200–13201.
99. Qu LT, Liu Y, Baek JB, Dai LM. Nitrogen-doped graphene as efficient metal-free electrocatalyst for oxygen reduction in fuel cells. *ACS Nano* 2010, 4:1321–1326.
100. Zhang LP, Xia ZH. Mechanisms of oxygen reduction reaction on nitrogen-doped graphene for fuel cells. *J Phys Chem C* 2011, 115:11170–11176.
101. Li YJ, Gao W, Ci LJ, Wang CM, Ajayan P. Catalytic performance of Pt nanoparticles on reduced graphene oxide for methanol electro-oxidation. *Carbon* 2009, 48:1124–1130.
102. Xin YC, Liu JG, Zhou Y, Liu WM, Gao JA, Xie Y, Yin Y, Zou ZG. Preparation and characterization of Pt supported on graphene with enhanced electrocatalytic activity in fuel cell. *J Power Sources* 2010, 196:1012–1018.
103. Li YM, Tang LH, Li JH. Preparation and electrochemical performance for methanol oxidation of Pt/graphene nanocomposites. *Chem Commun* 2009, 11:846–849.
104. Bong S, Kim YR, Kim I, Woo S, Uhm S, Lee J, Kim H. Graphene supported electrocatalysts for methanol oxidation. *Electrochem Commun* 2010, 12:129–131.
105. Jha N, Jafri RI, Rajalakshmi N. Graphene-multi walled carbon nanotube hybrid electrocatalyst support material for direct methanol fuel cell. *Int J Hydrogen Energy* 2011, 36:7284–7290.
106. Dong L, Gari RRS, Li Z, Craig MM, Hou S. Graphene-supported platinum and platinum-ruthenium nanoparticles with high electrocatalytic activity for methanol and ethanol oxidation. *Carbon* 2010, 48:781–787.
107. Shang N, Papakonstantinou P, Wang P, Silva SRP. Platinum integrated graphene for methanol fuel cells. *J Phys Chem C* 2010, 114:15837–15841.